

A Double Main Sequence in the Globular Cluster NGC 6397 ¹

A. P. Milone^{2,3}, A. F. Marino⁴, G. Piotto^{5,6}, L. R. Bedin⁷, J. Anderson⁷, A. Aparicio^{2,3}, S. Cassisi⁸, R. M. Rich⁹

ABSTRACT

High-precision multi-band *HST* photometry reveals that the main sequence (MS) of the globular cluster NGC 6397 splits into two components, containing $\sim 30\%$ and $\sim 70\%$ of the stars. This double sequence is consistent with the idea that the cluster hosts two stellar populations: (*i*) a primordial population that has a composition similar to field stars, and containing $\sim 30\%$ of the stars, and (*ii*) a second generation with enhanced sodium and nitrogen, depleted carbon and oxygen, and a slightly enhanced helium abundance ($\Delta Y \sim 0.01$). We examine the color difference between the two sequences across a variety of color baselines and find that the second sequence is anomalously faint in m_{F336W} . Theoretical isochrones indicate that this could be due to NH depletion.

Subject headings: globular clusters: individual (NGC 6397) — stars: Population II

²Instituto de Astrofísica de Canarias, E-38200 La Laguna, Tenerife, Canary Islands, Spain; [milone,aparicio]@iac.es

³Department of Astrophysics, University of La Laguna, E-38200 La Laguna, Tenerife, Canary Islands, Spain

⁴Max Planck Institute for Astrophysics, Postfach 1317, D-85741 Garching, Germany; amarino@MPA-Garching.MPG.DE

⁵Dipartimento di Astronomia, Università di Padova, Vicolo dell'Osservatorio 3, Padova I-35122, Italy; giampaolo.piotto@unipd.it

⁶INAF-Osservatorio Astronomico di Padova, Vicolo dell'Osservatorio 5, I-35122 Padua, Italy

⁷Space Telescope Science Institute, 3800 San Martin Drive, Baltimore, MD 21218; [jander,bedin]@stsci.edu ²

⁸INAF-Osservatorio Astronomico di Collurania, via Mentore Maggini, I-64100 Teramo, Italy; cassisi@oa-teramo.inaf.it

⁹Division of Astronomy and Astrophysics, University of California, Los Angeles, 430 Portola Plaza, Box 951547, Los Angeles, CA 90095-1547, USA; rmr@astro.ucla.edu

1. Introduction

Globular clusters (GCs) were once thought to be composed of stars of a single composition and a single age, with few exceptions (such as ω Centauri). It had long been known that most clusters contained red-giant stars with anomalies in their light-element abundances (Kraft 1979), but it was not clear whether this came as a result of internal mixing or a variation in the primordial abundances.

High-resolution spectroscopy (e. g. Ramirez & Cohen 2002, Carretta et al. 2009) has shown that these abundance anomalies in the giants almost usually manifest themselves as an anticorrelation between Na and O abundances, which is indicative of contamination from high-temperature hydrogen-burning products (Denisenkov & Denisenkova 1989). A similar anticorrelation has also been observed in some un-evolved main-sequence (MS) stars (Gratton et al. 2001, Ramirez & Cohen 2002), where the internal temperatures do not allow hot CNO-cycle burning. This fact suggested the presence of two stellar generations in the some cluster.

Indeed, high-precision photometry from *Hubble Space Telescope* (*HST*) images has shown that ω Centauri and NGC 2808 host multiple distinct MSs (Anderson 1997, Bedin et al. 2004, Piotto et al. 2007), which have been associated with stellar populations with different helium (Norris 2004, D’Antona et al. 2005, Piotto et al. 2005), with the bluer MSs having a higher He-content than the redder ones (Norris 2004, Piotto et al. 2005, D’Antona et al. 2005). More recently, a split MS has been observed also in 47 Tucanae and NGC 6752 (Anderson et al. 2009, Milone et al. 2010, 2011a). Stellar evolutionary models predict that H-burning at high temperatures through the CNO cycle should result in enhanced production of He. In addition to He, such models also predict enhanced production of N, and Na and depletion of C, and O. This pattern of enhancement/depletion has recently been confirmed among the blue and red MS stars in NGC 2808 by Bragaglia et al. (2010).

Multiple populations have also been identified in the color-magnitude diagram (CMD) of some clusters in the form of multiple sub-giant branches (SGBs, Milone et al. 2008, Marino et al. 2009) or multiple or anomalously wide red-giant branches (RGBs, Marino et al. 2008, Yong et al. 2008, Lee et al. 2009). Multiple populations with discrete helium abundance may also offer an explanation for the complex HB morphology exhibited by some clusters

¹Based on observations with the NASA/ESA *Hubble Space Telescope*, obtained at the Space Telescope Science Institute, which is operated by AURA, Inc., under NASA contract NAS 5-26555.

²Since July 18th 2011 at INAF-Osservatorio Astronomico di Padova, Vicolo dell’Osservatorio 5, I-35122 Padova, Italy, EU.

(Busso et al. 2007, D’Antona & Caloi 2008, Catelan, Valcarce & Sweigart 2009). A direct confirmation of a connection of the HB shape with the chemical content of HB stars comes from Marino et al. (2011), who have found that stars on the blue side of the instability strip of the cluster M4 are Na-rich and O-poor, whereas stars on the red HB are all Na-poor.

In this paper, we present a study of multiple stellar populations in the nearby GC NGC 6397. Evidence for a large spread in light-elements abundance, and a clear Na-O anticorrelation in this GC have been extensively documented in literature (Bell et al. 1979, Briley et al. 1990, Pasquini et al. 2004, Gratton et al. 2001, Carretta et al. 2005, 2009, Lind et al. 2009, 2011, L11). Recently, Richer et al. (2006) used the Advanced Camera for Surveys (ACS) of the *HST* for 126 orbits to image an outer region of NGC 6397 in the F606W and F814W bands. The spectacular CMD they obtained reaches the deepest intrinsic luminosities for a GC achieved thus far, and reveals an extremely tight MS in the $m_{F606W} - m_{F814W}$ color system (Anderson et al. 2008a). These observations are consistent with negligible He variation among NGC 6397 stars: $\Delta Y < 0.02$ (Di Criscienzo et al. 2009). Here, we take advantage of the multi-band *HST* photometry of the central region to study the MS of NGC 6397 for signs of multiple populations. The paper is organized as follows. The data and the data reduction are described in Sect. 2, results are shown in Sect. 3, and discussed in Sect. 4.

2. Observations and data reduction of NGC 6397

For this project we used *HST* images taken at three different epochs with the Wide Field Channel of the ACS (ACS/WFC) and the ultraviolet/visible channel of the Wide-Field Camera 3 (WFC3/UVIS). In particular, we used the following data sets (program-ID, camera, date, filters, number of exposures, exposure time): (1) GO-11633, WFC3/UVIS, March 2010, F336W, 6×620 s and F225W, 22×680 s; (2) GO-10257, ACS/WFC, August 2004-June 2005, F435W, 5×13 s + 5×340 s; (3) GO-10775, ACS/WFC, May 2006, F606W, 1 s +4×15 s and F814W, 1 s +4×15 s. The field covered by these images is centered on the cluster core. Their footprint are shown in Fig. 1, together with an image of the 10×10 arcsec central field taken through the F814W filter. Clearly, crowding is not severe, even in the center of this nearby cluster.

Star positions and fluxes in the ACS/WFC images were measured with the software described by Anderson et al. (2008b). The program analyzes a set of exposures simultaneously in order to produce a catalogue of stars over the field of view. Stars are measured in each image independently by means of a spatially variable point-spread-function model from Anderson & King (2006), plus a spatially constant perturbation of the PSF that accounts

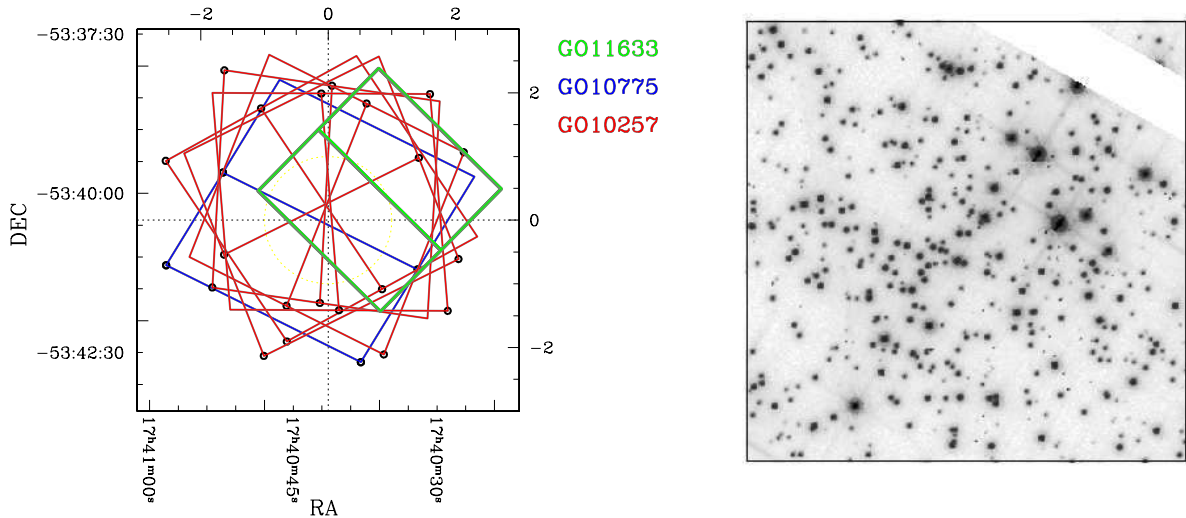


Fig. 1.— *Left panel:* Footprint of the *HST* data sets used in this paper. The small circles mark the corner of the WFC chip #1. *Right panel:* 10×10 arcsec field of a single F814W image centered on the cluster center.

for the effects of focus variations. The photometry has been calibrated as in Bedin et al. (2005) using the encircled energy and zero points of Sirianni et al. (2005).

The WFC3/UVIS images were reduced with a software that is adapted from `img2xym_WFI` (Anderson et al. 2006). Astrometry and photometry were corrected for pixel area and geometric distortion as in Bellini, Anderson & Bedin (2011). The proper motions were derived as in Milone et al. (2006).

This paper is mainly based on high-precision photometry, and is limited to a sub-sample of stars that are relatively isolated, are well-fit by the PSF, and also have small photometric and astrometric errors. The photometric software provides a number of quality indices that can be used as diagnostics of the reliability of photometric measurements. Specifically, these are: (1) the rms of the positions measured in different exposures transformed in a common reference frame (rms_X and rms_Y), (2) the residuals to the PSF fit for each star (q), and (3) the ratio between the estimated flux of the star in a 0.5 arcsec aperture and the flux from neighbouring stars within the same aperture (o , see Anderson et al. 2008b for details.) To select this high-precision sub-sample of stars, we followed the procedure described by Milone et al. (2009, Sect. 2.1) and illustrated in the upper panels of Fig. 2 for NGC 6397. As an example, in the lower panels we show the m_{F336W} vs. $m_{F336W} - m_{F435W}$ CMD of all the measured stars, of rejected stars, and of stars that pass the adopted criteria of selection. Since NGC 6397 ($l \simeq 338^\circ$, $b \simeq -12^\circ$) is located in a Galactic field richly populated by Bulge

and disk stars, we must make every effort to remove from our final list stars that do not belong to the cluster.

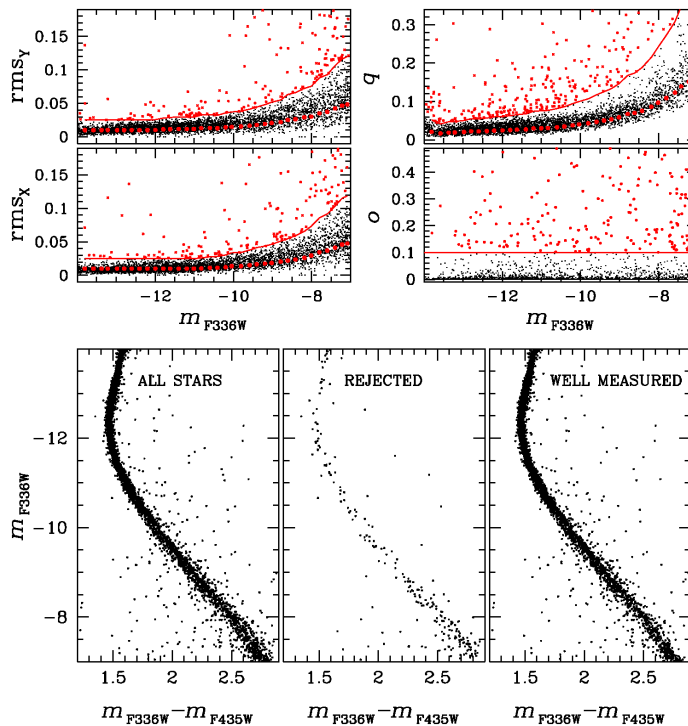


Fig. 2.— *Upper panels:* Diagnostic parameters used to select the stars with the best photometry are plotted as a function of m_{F336W} . Red lines separate the well measured stars (thin black points) from those that are more likely to have a poorer photometry (red thick points). *Lower panels:* Comparison of the CMD of all the measured stars (left), of rejected stars (middle), and of stars that pass our criteria of selection (right).

We measured proper motions using the F435W images of GO-10257 data set and the GO-10775 images, collected in two epochs separated by ~ 2 years. Figure 3 shows the vector-point diagram of proper motions. The separation between field stars and cluster stars is very well defined and cluster members were selected on the basis of their common proper motion. In all CMDs discussed in the following, field stars have been removed using the proper motion selection criterion.

The average reddening for NGC 6397 is $E(B - V) = 0.18$ (Harris 1996, 2010). Usually, such a large reddening is not uniform across an ACS field. A visual inspection at the CMDs of NGC 6397 indeed reveals that the sequences are broadened by differential reddening. We corrected the effect of differential reddening by means of a procedure that is described in detail in Milone et al. (2011b), and used in many other papers by these authors.

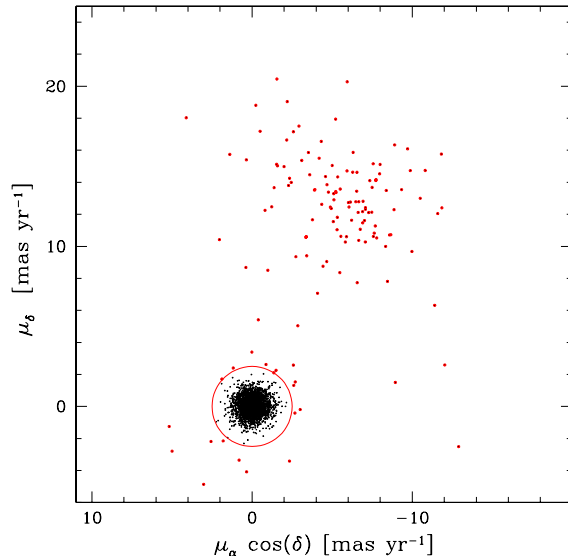


Fig. 3.— Vector-point diagram of the proper motions in equatorial coordinates. The red circle separates cluster members (black points) from field objects (red points).

Briefly, we define the fiducial MS ridge-line in a given color system for the cluster and estimate, for each star, how the observed stars in its vicinity may systematically lie to the red or to the blue of the fiducial sequence; this systematic color and magnitude offset, measured along the reddening line, is indicative of the local differential reddening.

We find that the reddening variations are typically smaller than $\Delta E(B-V) \sim 0.01$ mag, and never exceed 0.026 mag. The reddening map we obtained is plotted in Fig. 4, where we divide the field of view into 8 horizontal slices and 8 vertical slices, and plot $\Delta E(B-V)$ as a function of the Y (upper Panels) and X coordinate (right Panels). We have also divided the whole field of view into 32×32 boxes and calculated the average $\Delta E(B-V)$ within each of them. The resulting reddening map is shown in the lower-left Panel, where each box is represented as a gray square. The levels of gray are indicative of the amount of differential reddening as shown in the upper-right plot. As an example, a comparison of the original m_{F336W} vs. $m_{F336W} - m_{F435W}$ CMD is provided in Fig. 5.

3. The split Main Sequence

Figure 6 shows CMDs with two different color baselines: m_{F336W} vs. $m_{F225W} - m_{F336W}$ and m_{F336W} vs. $m_{F336W} - m_{F435W}$. It is clear that the MS of NGC 6397 is split into two distinct sequences in both diagrams. It is interesting to note that in the $m_{F225W} - m_{F336W}$

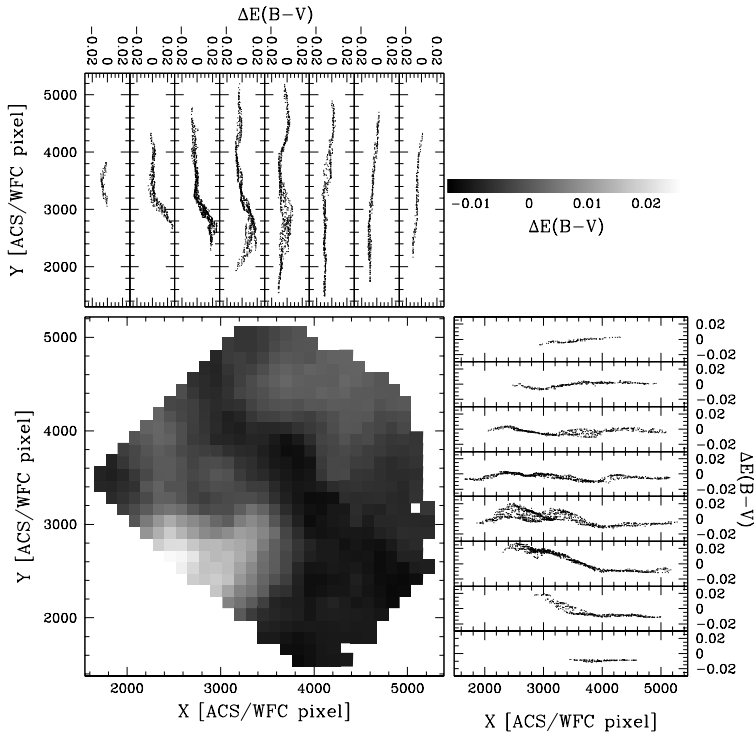


Fig. 4.— *Bottom-left*: Map of differential reddening in the NGC 6397 field of view. The gray levels correspond to the magnitude of the variation in local reddening, as indicated in the upper-right panel. We also divided the field of view into 8 horizontal slices and 8 vertical slices. *Upper-left* and *lower-right* panels show $\Delta E(B - V)$ as a function of the Y and X coordinates in each slice.

color, the majority of the stars are on the blue MS branch (hereafter MSb), while in the $m_{F336W} - m_{F435W}$ color system, the majority of stars are on the redder sequence. We will explore and quantify this effect below.

The presence of a split MS is even more evident from the two-color diagram shown in the right panels. We have separated the two sequences into a MSa (green colors in the right upper panel of Fig. 6), and a MSb (magenta colors).

The insets of left and middle panel of Fig. 6 show that the two MSs appear to merge close to the turn-off, and that the turn-off/subgiant-branch part of the CMD is narrow and well defined, implying that any age difference between the two populations must be less than a few 100 Myrs. Putting a better upper limit on the possible age spread will require a measurement of the overall C+N+O content for the stars in the two populations. We note that the narrow magnitude distribution of SGB stars rules out the possibility that the double MS could be due to residual spatial variations of reddening that are beyond the sensitivity

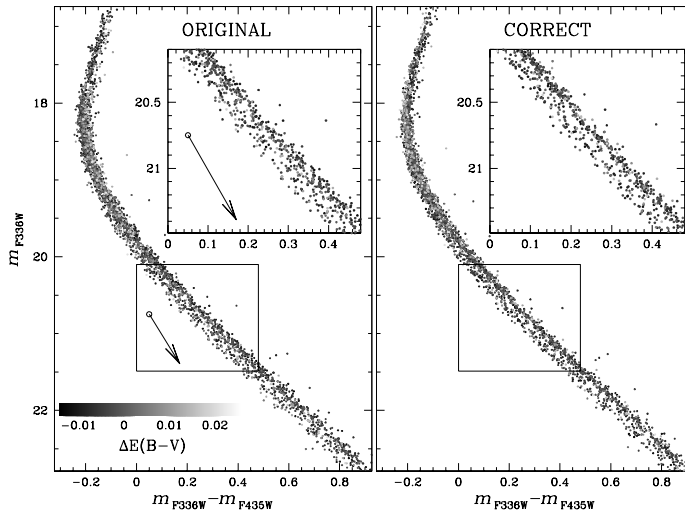


Fig. 5.— Comparison of the original (left panel) and the differential reddening corrected (right panel) m_{F336W} vs. $m_{F336W} - m_{F435W}$ CMD. The insets show a zoom around the MS while the arrows indicate the reddening direction. The gray levels corresponds to different differential reddening variation as indicated in the figure.

of the method that we used to correct them, as the reddening line is nearly perpendicular to the SGB sequence.

There is additional evidence that the MS splitting is real. First of all, the two MSs are visible everywhere in the field. Furthermore, reddening would move stars in the same direction in any CMDs (e. g. higher reddening would move stars towards redder colors and fainter magnitudes, at odds with the observed behaviour of the MSa and MSb, which invert their relative position in different CMDs of Fig. 6.)

The upper-left panel of Figure 7 shows the distribution of MSa and MSb stars in the proper motion vector-point diagram, with the colors that were assigned in Fig. 6. The two samples show no difference in their proper-motion distributions. To more quantitatively test this, in the upper-right panel we show the cumulative distribution of proper motions. A Kolmogorov-Smirnov test shows a very high probability (P=66%) for the null hypothesis that the two populations have a similar proper-motion distributions. The spatial distribution is plotted in the lower-left panel. In this case, as well, the Kolmogorov-Smirnov test indicates that there is no evidence for difference in the radial distributions (P=67%).

In order to estimate the fraction of stars in each MS we followed the procedure illustrated in Fig. 8, which has already been used in several previous papers (e. g. Piotto et al. 2007). The left panel shows the same m_{F336W} vs. $m_{F336W} - m_{F435W}$ CMD of Fig. 6, zoomed around

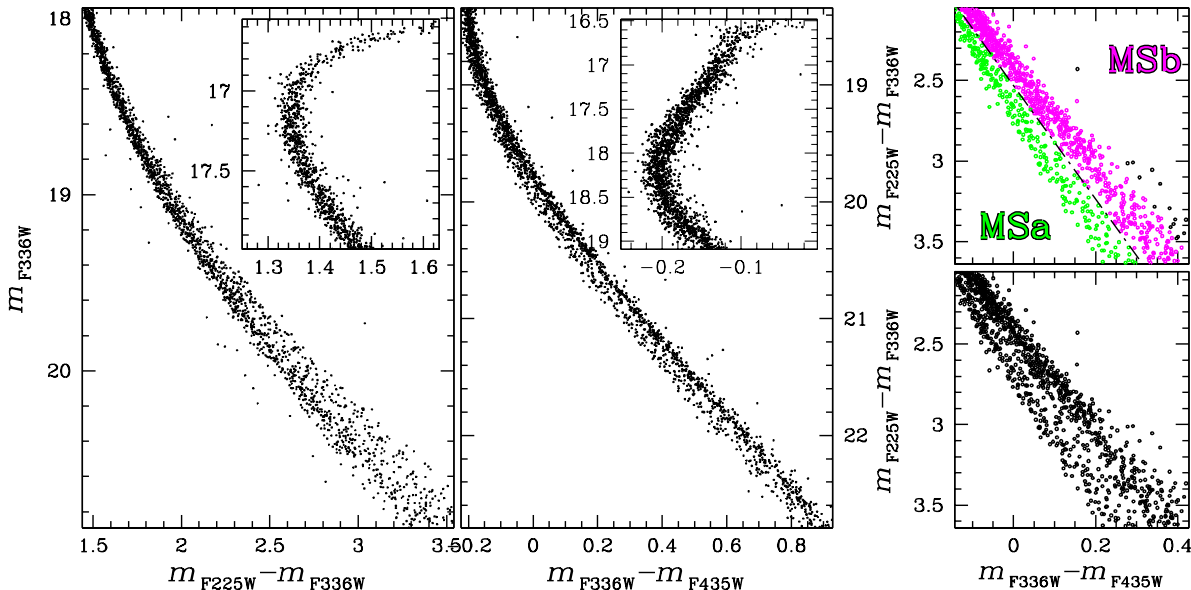


Fig. 6.— *Left panels:* Proper-motion-selected, differential-reddening-corrected m_{F336W} vs. $m_{\text{F225W}} - m_{\text{F336W}}$ (*left panel*) and m_{F336W} vs. $m_{\text{F336W}} - m_{\text{F435W}}$ (*middle panel*) CMDs for MS stars in NGC 6397. The insets show a zoom of the SGB region. *Right panels:* the $m_{\text{F225W}} - m_{\text{F336W}}$ vs. $m_{\text{F336W}} - m_{\text{F435W}}$ two-color diagram for MS stars with $19.2 < m_{\text{F336W}} < 20.6$. The dot-dashed line in the upper panel was drawn by hand to separate the MSa and MSb stars, plotted green and magenta, respectively.

the upper MS region, where the split is most evident. The red line is the fiducial ridge line of MSb. To determine it, we started by selecting a sample of MSb stars by means of a hand-drawn first-guess ridge line, and choosing the stars within a limited color range about this line. We then calculated the median color and magnitude of MSb stars in intervals of 0.2 magnitude in F336W, interpolated these median points with a spline, and did an iterated sigma-clipping of the straightened sequence. To obtain the straightened MS of the middle panel, we subtracted from the color of each star the color of the fiducial sequence at the F336W magnitude of the star. The color distribution of the points in the middle panel were analysed in four magnitude bins over the interval $19.6 < m_{\text{F336W}} < 20.6$. The distributions have two clear peaks, which we fit with two Gaussians (magenta for the MSb and green for the MSa). From the areas under the Gaussians, $71 \pm 3\%$ of stars turns out to belong to the MSb, and $29 \pm 3\%$ to the MSa. Within the statistical uncertainties these fractions are the same in all magnitude intervals.

Since we have photometry through five different *HST* filters, we can study the relative location of the two MSs of NGC 6397 in a variety of CMDs constructed using all possible combinations of the photometric bands, as shown in Fig. 9. The upper panels show the

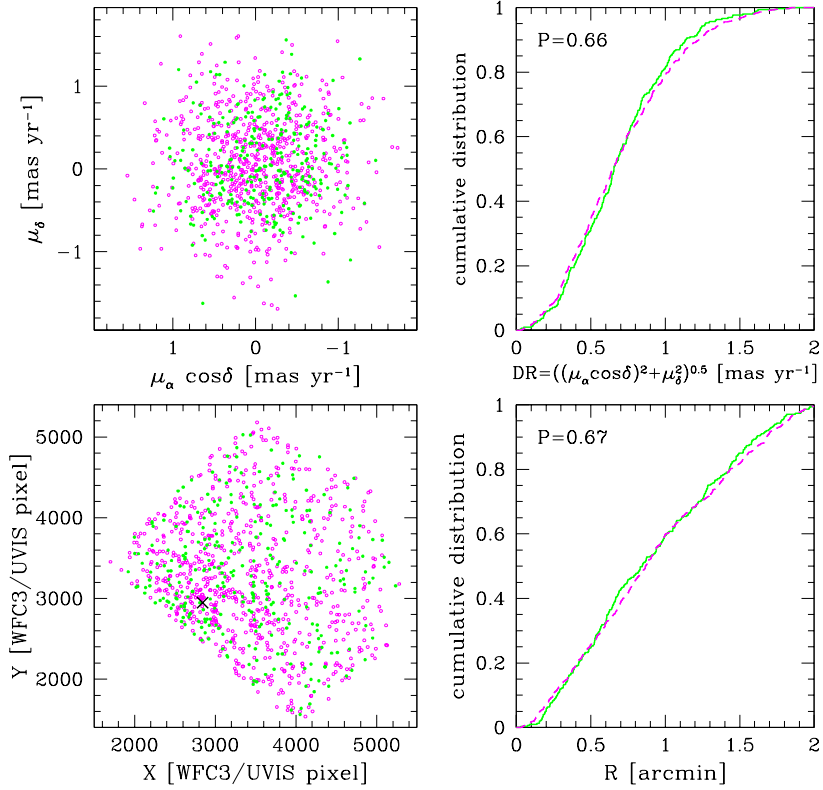


Fig. 7.— Upper panels: Distribution of MSA and MSb stars in the vector-point diagram of proper motions (right). The cumulative distributions is plotted in the left panel. Lower panels: Spatial distributions (left) and cumulative radial distributions of MSA and MSb stars.

CMDs m_{F336W} vs. $m_X - m_{F336W}$ or $m_{F336W} - m_X$ (where X represents F225W, F336W, F435W, F606W, F814W). We used the same color code to plot the MSA and MSb stars identified in the color-color diagram in Fig. 6. The MSA has a $m_{F225W} - m_{F336W}$ color that is redder than the MSb, but the relative color is opposite of this in all the other $m_{F336W} - m_X$ colors.

The lower panels of Fig. 9 show the m_{F814W} vs. $m_X - m_{F814W}$ CMDs. Here, the MSA is bluer than the MSb, with the exception of the already mentioned m_{F814W} vs. $m_{F336W} - m_{F814W}$ CMD. The separation of the two sequences increases for larger color baselines in the remaining CMDs. To better visualize the relative positions of the two MSs, in Fig. 10 we plotted the fiducials of the MSA and the MSb derived for each CMD of Fig. 9 following the same procedure above described.

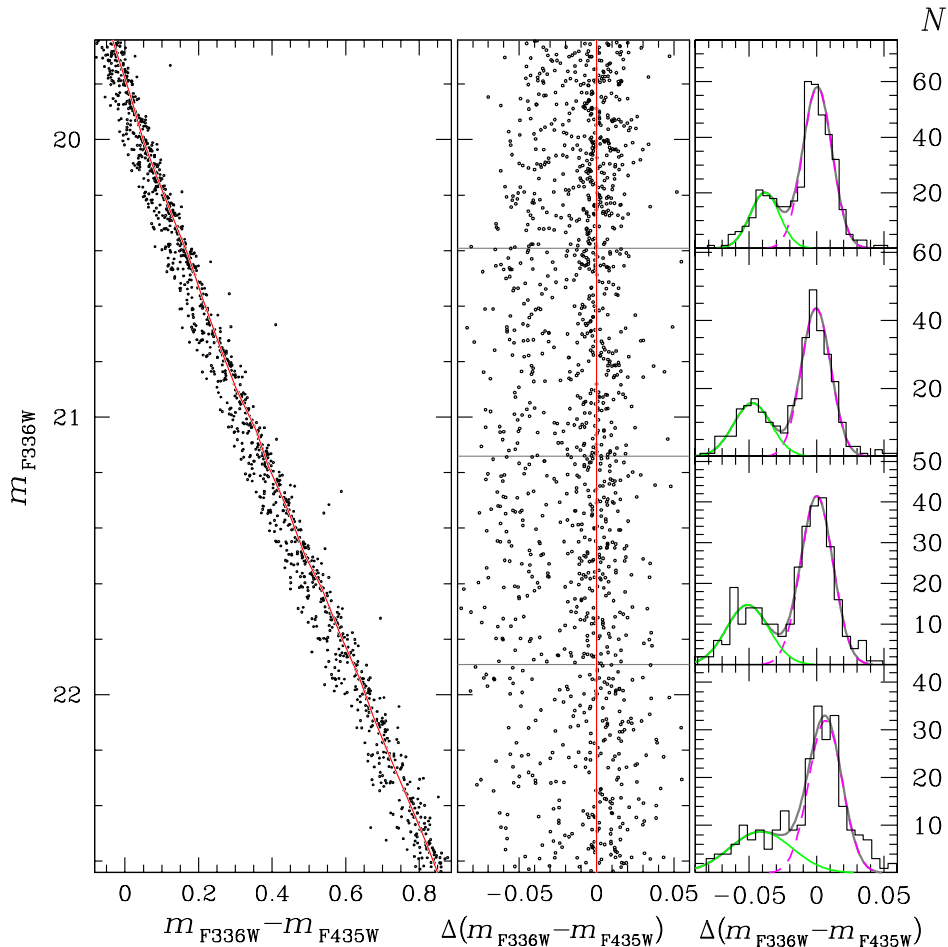


Fig. 8.— *Left panel:* A zoom of the region of the m_{F336W} vs. $m_{\text{F336W}} - m_{\text{F435W}}$ CMD from Fig. 6, where the MS split is more evident. The continuous line is a fiducial line of the MS. *Middle panel:* The same CMD, after subtraction of the color of the fiducial line. *Right panels:* The color distribution of the points in the middle panel in four F336W magnitude intervals. The continuous grey lines are fits by a sum of the two Gaussians.

4. Discussion

In this paper we have shown that the MS of NGC 6397 is clearly split into two distinct sequences. Broadened or multiple MSs have been observed in other clusters, including 47 Tuc, ω Centauri, NGC 2808, and NGC 6752 (Anderson 1997, Bedin et al. 2004, Piotto et al. 2007). In ω Centauri and NGC 2808 the multiple MSs have been associated with stellar populations that have large difference in their helium abundance, with the bluer MSs having a higher He-content than the redder ones (Norris 2004, Piotto et al. 2005, D’Antona et al. 2005). Stellar evolutionary models predict that H-burning at high temperatures through

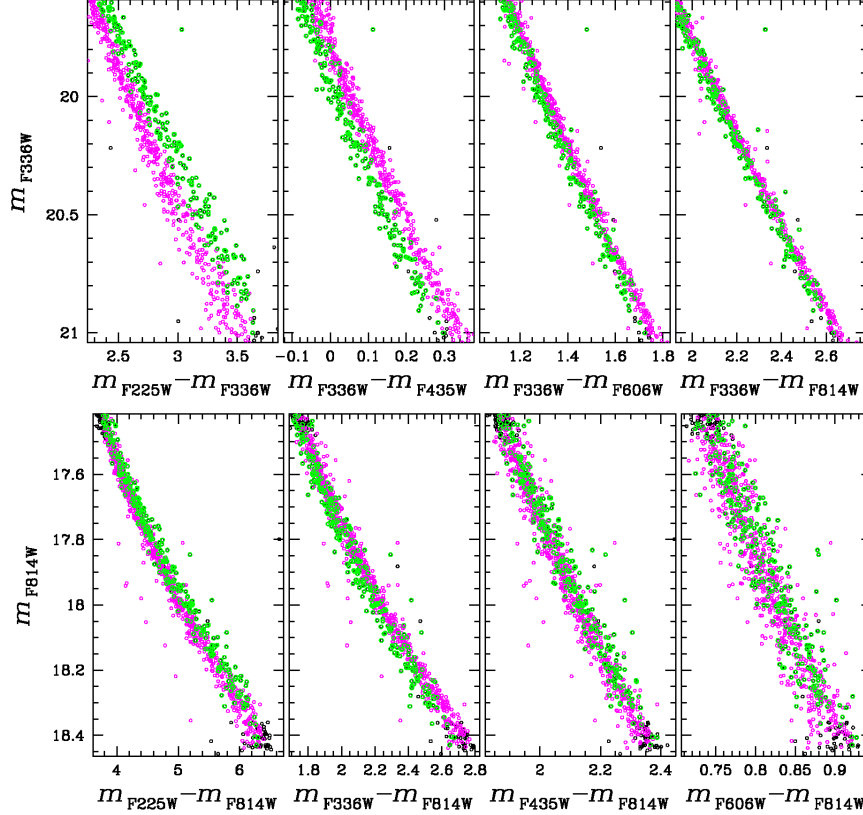


Fig. 9.— *Upper panels:* m_{F336W} vs. colors made with m_{F336W} and F225W, F435W, F606W, and F814W for MSa stars (green) and MSb stars (magenta). MSa is bluer than MSb in all the colors except $m_{F225W} - m_{F336W}$. *Lower panels:* m_{F814W} vs. colors made with m_{F814W} and F225W, F336W, F435W, and F606W. In these colors the MSa is redder than the MSb with the exception of the CMD based on the $m_{F336W} - m_{F814W}$ color.

the CNO cycle results in an enhanced production of He. In addition to He, such models also predict enhanced production of N, and Na and depletion of C, and O. This pattern of enhancement/depletion has recently been confirmed among the blue and red MS stars in NGC 2808 by Bragaglia et al. (2010).

Since the seventies, spectroscopic studies of NGC 6397 giants have shown that the RGB stars exhibit a large spread in their C and N abundances (Bell et al. 1979). Significant star-to-star variations in the Na content have also been detected among unevolved TO stars (Gratton et al. 2001, Lind et al. 2009), thus demonstrating that such abundance variations

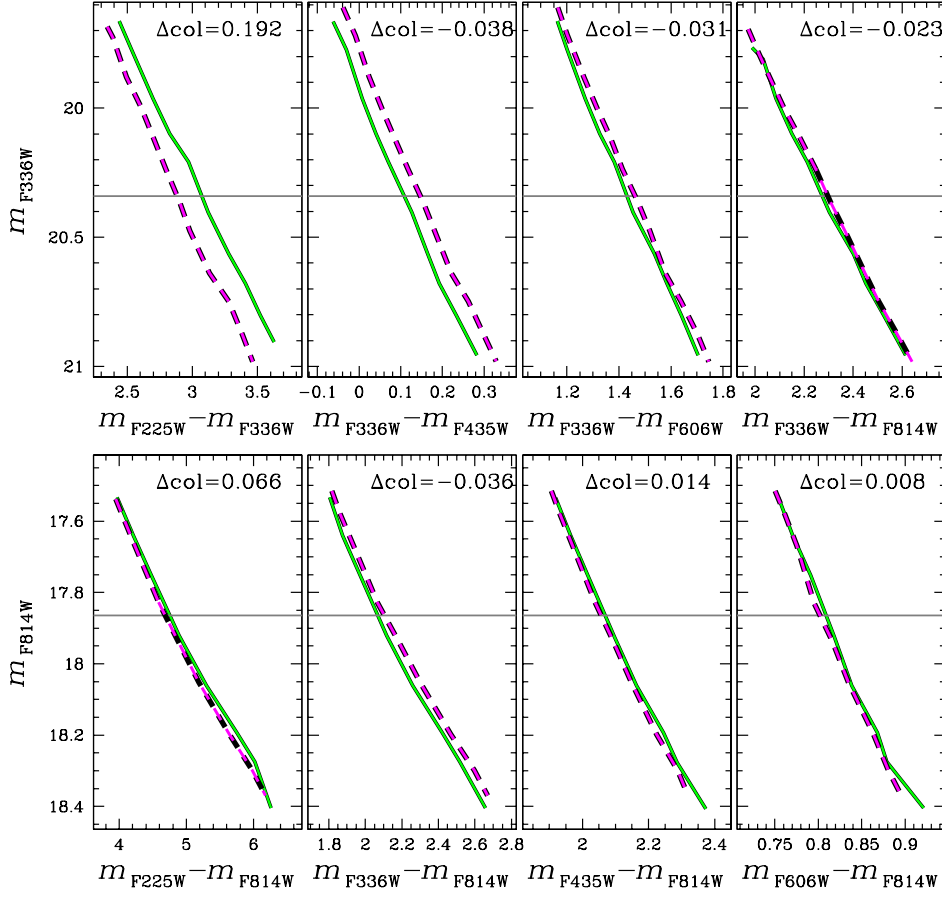


Fig. 10.— *Upper panels:* MS fiducials for the same CMDs shown in the upper panels of the previous figure. MSa is represented by the solid green line, and MSb by the dashed magenta line. We report at the top of each panel the color separation of the fiducials of MSa and MSb measured at the $m_{F336W} = 20.3$ level (indicated by the horizontal grey line). *Lower panels:* MS fiducials for the CMDs in the lower panels of the previous figure. The reported $\Delta(\text{col})$ values are calculated at $m_{F814W} = 17.9$.

must have an intrinsic (primordial) rather than an evolutionary origin. NGC 6397 stars also show Na-O anticorrelation (Carretta et al. 2005, 2009, L11). Even more relevant for the present discussion, L11 analysed the chemical composition of a large number of elements in 21 RGB stars of NGC 6397, and found that Na and O abundances have a bimodal distribution, with about the 75% of stars being enriched in Na and depleted in O, while the remaining $\sim 25\%$ of the stars have a abundance patterns similar to field stars. Similarly, Carretta et al. (2009) found that 30% of the stars in their sample are Na-poor/O-rich. L11 also demonstrated that the RGB of NGC 6397 is bimodal in the Strömgen color index $c_y = c_1 - (b - y)$, with the Na-poor and Na-rich stars populating the blue and red RGB

sequences, respectively. It is interesting to note that, in Sect. 3 we found that $71 \pm 3\%$ of the MS stars populate the MSb. This fraction is consistent with the 75% of Na-rich, O-poor stars found by L11. Therefore, we suggest a connection between the MSb and the Na-rich, O-poor population of NGC 6397. This would imply that the MSa represents the first generation, and its intermediate-mass stars polluted the cluster with gas rich in He, N, and Na to make the second generation, MSb.

In an effort to quantify the observed MS split, we have characterized the fiducial sequences by measuring the color difference between the MSa and MSb at the reference magnitude of $m_{\text{F814W}} = 17.9$ (Fig. 3). For an assumed apparent distance modulus of $(m - M)_{\text{F814W}} = 12.2$, this corresponds to an absolute magnitude of $M_{\text{F814W}} = 5.7$.

To compare these observations against expectations from synthetic photometry, we adopted the BaSTI isochrones (Pietrinferni et al. 2004) for the populations listed in Table 1, and determined T_{eff} and $\log g$ for MS stars at $M_{\text{F814W}} = 5.7$. We adopted the average C, N, and O abundance of N-poor stars as measured by Carretta et al. (2005) for dwarf and SGB stars in NGC 6397.

These temperatures and gravities (listed in Table 1) were then used to calculate model atmospheres with the ATLAS12 code (Kurucz 2005, Castelli 2005, Sbordone 2005), which allowed us to use specific chemical compositions. We then used the SYNTH code (Sbordone et al. 2007) to synthesize the spectrum from 1000Å to 10000Å and the resulting synthetic spectra were integrated over the transmission curve of each of our filters to produce the synthetic magnitudes and colors. We did this separately for an MSa star, using the composition listed in Table 1, and for an MSb star, using the three different composition options given in Table 1.

The left-panel of Fig. 11 shows a comparison of the observed $m_X - m_{\text{F814W}}$ color differences between MSa and MSb against the synthetic ones. The blue squares indicate the color differences corresponding to Option I, where we assumed for the two MSs the same C, N, O mixture, but different He content. There is a good agreement with the observed color differences in most bands, but a significant disagreement with the F336W band. We conclude that Helium alone cannot account for the observed MS split.

It is worth noting that Nitrogen mainly affects the F336W photometry via the NH band around $\lambda \sim 3400 \text{ \AA}$ (e. g. Marino et al. 2008). In Option II, we assume that the MSb stars in NGC 6397 are N-enhanced, but have the same He content. We assumed for the MSb the average C, N, and O abundance found by Carretta et al. (2005) for N-rich stars.

The colors that result from Option II are plotted as gray triangles in Fig. 11. There remains a significant discrepancy between the simulated and the observed color differences in

Table 1: Parameters used to simulate synthetic spectra of an MSa and an MSb star with $m_{F814W}=17.9$, for the three assumed options.

MS (Option)	T_{eff}	$\log g$	Y	[C/Fe]	[N/Fe]	[O/Fe]
MSa (all)	5373	3.26	0.246	0.10	-0.20	0.45
MSb (I)	5398	3.26	0.256	0.10	-0.20	0.45
MSb (II)	5373	3.26	0.246	-0.05	1.35	0.10
MSb (III)	5398	3.26	0.256	-0.05	1.35	0.10

the F336W and F225W bands, now in the opposite sense to that seen in Option I. Turning instead to Option III, with differences in both helium and the CNO elements, we see that the red asterisks in Fig. 11 are in better agreement with all of the observed color differences, yet it is still not perfect for the F336W filter.

A careful fine-tuning of the composition differences between the two MSs might remove the residual discrepancies between observed and theoretical points, but it is unclear whether that would tell us what is really going on without high-resolution spectra. The difference between the synthetic spectra of a MSa and a MSb stars as calculated for Option III is shown in the upper-right panel of Fig. 11, while the band-passes of our filters are plotted in the bottom-right panel.

In conclusion, the observed color differences between the two MSs are consistent with the presence of two populations with different helium and light-element content. Specifically, the MSa would correspond to the first stellar generation with primordial He, and O-rich/N-poor stars, while the MSb would be made of stars enriched in He and N but depleted in O. While the bluer MSs of ω Centauri and NGC 2808 imply extremely high He abundances (up to $Y\sim 0.38$), the MS of NGC 6397 is consistent with a significantly smaller helium enhancement of second-generation stars at a level of $\Delta Y=0.01$, as already suggested by Di Criscienzo et al. (2010). Note that we reached similar conclusions, based on the same technique described above, for 47 Tuc (Milone et al. 2011a) where we found a $\Delta Y\sim 0.02$.

Finally, we recall that light-element variations have been detected in all GCs studied to date (see Gratton et al. 2004 for a review). If the interpretation of the split MS of NGC 6397 given above is correct, then either multiple or spread MSs should be observed in most (all?) GCs. In this paper (and in a similar paper on 47 Tuc), we have demonstrated that the combination of UV and visual photometry, such as m_{F225W} , m_{F336W} , and m_{F435W} , is a powerful tool to isolate stellar populations in the color-magnitude and color-color diagrams, allowing us to infer their He and CNO content.

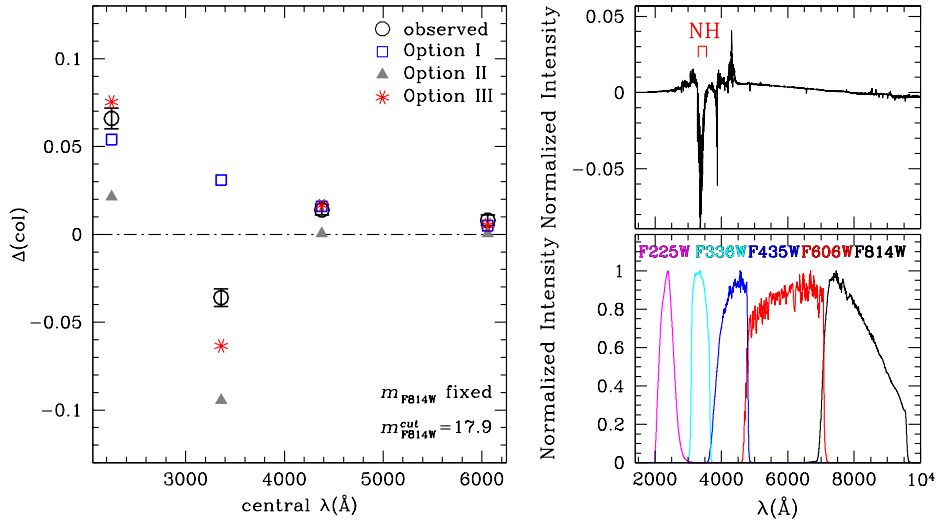


Fig. 11.— *Left panel:* Color differences of the fiducial lines of MSa and MSb. The adopted colors are $m_X - m_{F814W}$, where $X = F225W, F336W, F435W,$ and $F606W$. Each color difference is measured at $m_{F814W} = 17.9$, and is plotted as a function of the central wavelength of the filter X . Positive or negative Δcol values indicate that the MSa is bluer or redder than the MSb. *Upper-right panel:* The difference between the synthetic spectrum of a MSa and a MSb star (see text for more details). *Lower-right panel:* Normalized responses of the *HST* filters used in this paper.

G.P. and S.C. acknowledge partial support by PRIN INAF ‘Formation and Early Evolution of Massive Star Clusters’ and by ASI under the program ASI-INAF I/016/07/0. G.P. acknowledge partial support by the Universita’ di Padova with the Progetto di Ateneo ‘Multiple Stellar Populations in Star Clusters’. J.A. acknowledges the support of STScI grant GO-11233.

REFERENCES

- Anderson, A. J. 1997, Ph.D. Thesis, Univ. of California, Berkeley
- Anderson, J., & King, I. R. 2006, Instrument Science Report ACS 2006-01, 34 pages, 1
- Anderson, J., et al. 2008a, AJ, 135, 2114
- Anderson, J., et al. 2008b, AJ, 135, 2055
- Bedin, L. R., Piotto, G., Anderson, J., Cassisi, S., King, I. R., Momany, Y., & Carraro, G. 2004, ApJ, 605, L125
- Bedin, L. R., Cassisi, S., Castelli, F., Piotto, G., Anderson, J., Salaris, M., Momany, Y., & Pietrinferni, A. 2005, MNRAS, 357, 1038
- Bell, R. A., Dickens, R. J., & Gustafsson, B. 1979, ApJ, 229, 604
- Bellini, A., Anderson, J., & Bedin, L. R. 2011, PASP, 123, 622
- Briley, M. M., Bell, R. A., Hoban, S., & Dickens, R. J. 1990, ApJ, 359, 307
- Bragaglia, A., et al. 2010, ApJ, 720, L41
- Busso, G., Cassisi, S., Piotto, G., Castellani, M., Romaniello, M., Catelan, M., Djorgovski, S. G et al. 2007, A&A, 474, 105;
- Carretta, E., Gratton, R. G., Lucatello, S., Bragaglia, A., & Bonifacio, P. 2005, A&A, 433, 597
- Carretta, E., et al. 2009a, A&A, 505, 117
- Catelan, M., Valcarce, A. A. R., & Sweigart, A. V. 2010, IAU Symposium, 266, 281
- D’Antona, F., & Caloi, V. 2004, ApJ, 611, 871
- D’Antona, F., Bellazzini, M., Caloi, V., Pecci, F. F., Galleti, S., & Rood, R. T. 2005, ApJ, 631, 868
- Denisenkov, P. A., & Denisenkova, S. N. 1989, Astronomicheskij Tsirkulyar, 1538, 11
- D’Ercole, A., Vesperini, E., D’Antona, F., McMillan, S. L. W., & Recchi, S. 2008, MNRAS, 391, 825
- di Criscienzo, M., D’Antona, F., & Ventura, P. 2010, A&A, 511, A70

- Gratton, R. G., et al. 2001, *A&A*, 369, 87
- Gratton, R., Sneden, C., & Carretta, E. 2004, *ARA&A*, 42, 385
- Harris, W. E. 1996, *AJ*, 112, 1487
- Kraft, R. P. 1979, *ARA&A*, 17, 309
- Lee, J.-W., Kang, Y.-W., Lee, J., & Lee, Y.-W. 2009, *Nature*, 462, 480
- Lind, K., Primas, F., Charbonnel, C., Grundahl, F., & Asplund, M. 2009, *A&A*, 503, 545
- Lind, K., Charbonnel, C., Decressin, T., Primas, F., Grundahl, F., & Asplund, M. 2011, *A&A*, 527, A148 (L11)
- Marino, A. F., Villanova, S., Piotto, G., Milone, A. P., Momany, Y., Bedin, L. R., & Medling, A. M. 2008, *A&A*, 490, 625
- Marino, A. F., Milone, A. P., Piotto, G., Villanova, S., Bedin, L. R., Bellini, A., & Renzini, A. 2009, *A&A*, 505, 1099
- Marino, A. F., Villanova, S., Milone, A. P., Piotto, G., Lind, K., Geisler, D., & Stetson, P. B. 2011b, *ApJ*, 730, L16
- Milone, A. P., Villanova, S., Bedin, L. R., Piotto, G., Carraro, G., Anderson, J., King, I. R., & Zaggia, S. 2006, *A&A*, 456, 517
- Milone, A. P., et al. 2008, *ApJ*, 673, 241
- Milone, A. P., Bedin, L. R., Piotto, G., & Anderson, J. 2009, *A&A*, 497, 755
- Milone, A. P., et al. 2010, *ApJ*, 709, 1183
- Milone, A. P., Piotto, G., Bedin, L. R., et al. 2011a, *A&A*, in press (arXiv:1108.2391)
- Milone, A. P., Piotto, G., Bedin, L. R., et al. 2011b, *ApJ*, in press (arXiv:1109.0900)
- Norris, J. E. 2004, *ApJ*, 612, L25
- Pasquini, L., Bonifacio, P., Randich, S., Galli, D., & Gratton, R. G. 2004, *A&A*, 426, 651
- Piotto, G., et al. 2005, *ApJ*, 621, 777
- Piotto, G., et al. 2007, *ApJ*, 661, L53
- Ramírez, S. V., & Cohen, J. G. 2002, *AJ*, 123, 3277

Richer, H. B., et al. 2006, *Science*, 313, 936

Sirianni, M., et al. 2005, *PASP*, 117, 1049

Yong, D., Grundahl, F., Johnson, J. A., & Asplund, M. 2008, *ApJ*, 684, 1159